

A shell element for finite strain analyses. Hyperelastic material models

Rita G. Toscano and Eduardo N. Dvorkin
Center for Industrial Research, TENARIS
Dr. Simini 250
2804, Campana, Argentina

Abstract

Purpose

To develop a simple and efficient shell element for large strains hyperelastic analyses.

Approach

Based on the classical MITC4 shell element formulation a 3D shell element with finite strain kinematics is developed. The new quadrilateral shell element has 5 d.o.f. per node and two global d.o.f. to model the thickness stretching. The shell element is implemented for hyperelastic material models and the application of different hyperelastic constitutive relations is discussed.

Practical Implications

The results obtained considering three of the hyperelastic material models available in the literature are quite different when the developed strains are relatively high; this indicates that, for analyzing actual engineering examples, experimental data should be used to decide on the most suitable constitutive relation.

Originality

The 3D version of the MITC4 element was developed

Keywords

shells; finite elements; hyperelasticity; finite strains;

1 Introduction

In 1970, Ahmad, Irons and Zienkiewicz presented a shell element formulation that after many years still constitutes the basis for modern finite element analysis of shell structures [1]. The original formulation was afterwards extended to material and geometric nonlinear analysis under the constraint of the infinitesimal strains assumption [2] - [4].

The fundamental features of the A-I-Z shell element are:

- Using isoparametric interpolation functions the displacements inside the shell element are interpolated from three displacement-d.o.f. and two rotation-d.o.f. at each node.
- The interpolated generalized displacement fields present C^0 continuity.
- The element is not based on any plate/shell theory but it is a continuum element incorporating several assumptions that we list below (degenerated solid element).

Kinematic and constitutive assumptions:

1. A straight line that is initially normal to the mid-surface remains straight after the deformation.
2. A straight line that is initially normal to the mid-surface is not stretched during the deformation.
3. The through-the-thickness stresses are zero.

It is important to remark that the second assumption precludes the consideration of finite strain deformations.

Even though the A-I-Z shell element was a breakthrough in the field of finite element analysis of shell structures, it suffers from the locking phenomenon and much research effort has been devoted to the development of A-I-Z type elements that do not present this problem [5]-[9]-[10].

The MITC4 shell element [11]-[13] which was developed to overcome the locking problem of the A-I-Z shell elements has become, since its development in the early eighties, the standard shell element for many finite element codes. However, the limitation of infinitesimal strains is still present in the MITC4 formulation.

Many researchers have developed shell elements that can model finite strain situations, among them:

- An early contribution by Rodal and Witmer [14], where after the displacement calculation the shell element thickness is updated neglecting the elastic strains and invoking the incompressibility of the plastic flow.
- In 1983 Hughes and Carnoy [15] developed a finite strain shell element for the Mooney-Rivlin material model which uses a plane-stress constitutive relation for the laminae and updates afterwards the thickness in a staggered iterative formulation.
- Simo and co-workers [16]-[20] in the period 1988-1992 developed a complete 3D nonlinear shell element formulation.
- Ramm and co-workers [21]-[22] developed 3D shell elements considering also through-the-thickness stretching.

In 1995 Dvorkin, Pantuso and Repetto developed the MITC4-TLH element, that based on the original MITC4 formulation can model finite strain elasto-plastic deformations [23]-[24]. This element imposes the condition of zero transversal stresses and its computational cost is rather high.

In the present paper we present an element that is also based on the MITC4 formulation and can efficiently model finite strain deformations using a general 3D material model.

The most relevant differences with the original MITC4 formulation are:

- For each quadrilateral element we have 22 d.o.f.: 5 generalized displacements per node plus 2 extra d.o.f. to incorporate the through-the-thickness stretching.
- We use a general 3D constitutive relation instead of the original laminae plane stress constitutive relation.

There are many hyperelastic constitutive models available in the literature. In order to explore the differences in their responses we implemented, for the new MITC4-3D shell element, three simple isotropic hyperelastic constitutive relations and we analyzed their responses for a number of finite strain cases.

2 The MITC4-3D formulation

Some of the basic features of our MITC4-3D element are:

1. The shell geometry is interpolated using mid-surface nodes and director vectors.
2. The nodal displacements and transverse shear strains are interpolated using the original MITC4 formulation [11].
3. For interpolating the director vectors special care is taken to avoid spurious director vector stretches [17] [25].
4. Two additional degrees of freedom are considered to include a linear thickness stretching. These thickness-stretching degrees of freedom are condensed at the element level.

2.1 Shell element geometry in the reference configuration

Following the MITC4 formulation we define, in the reference configuration, nodes on the shell mid-surface and at each node we define a *director vector* which represents, at that node, an approximation to the shell mid-surface [26].

Therefore, defining inside the element the natural coordinate system (r, s, t) [8], for the element shown in Fig. 1 with constant thickness we can write,

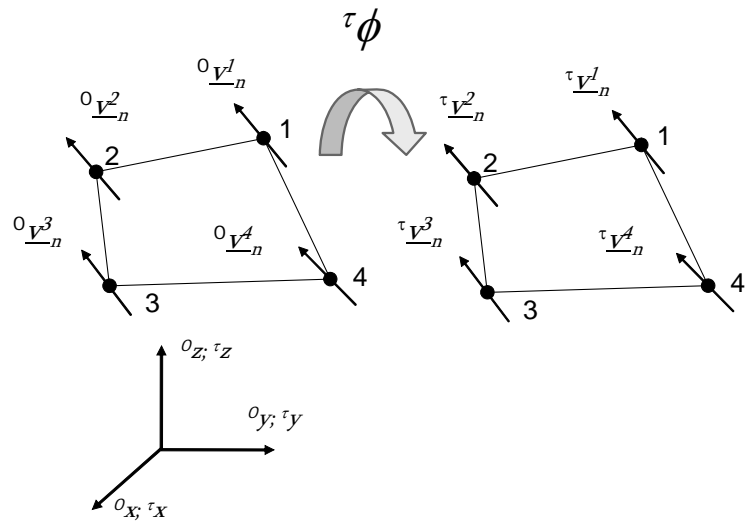


Figure 1: Reference ($t = 0$) and spatial ($t = \tau$) configurations

$${}^o \underline{x}(r, s, t) = h_k(r, s) {}^o \underline{x}_k + \frac{t}{2} {}^o \underline{d} a \quad (1a)$$

where [17] [25],

$${}^o \underline{d} = \frac{h_k(r, s) {}^o \underline{V}_n^k}{\left\| h_k(r, s) {}^o \underline{V}_n^k \right\|} \quad (1b)$$

and,

$h_k(r, s)$: isoparametric 2D interpolation functions [8],

${}^o \underline{x}_k$: k -node position vector,

a : constant element thickness.,

${}^o \underline{V}_n^k$: k -node director vector; with $\left\| {}^o \underline{V}_n^k \right\| = 1$.

In the above equations and in what follows we use the summation convention.

2.2 Shell geometry in the spatial configuration

For interpolating the spatial geometry in the τ -configuration, Fig. 1, we use,

$${}^\tau \underline{x}(r, s, t) = h_k(r, s) {}^\tau \underline{x}_k + \frac{t}{2} ({}^\tau \lambda_o + {}^\tau \lambda_1 t) {}^\tau \underline{d} a \quad (2a)$$

$${}^\tau \underline{d} = \frac{h_k(r, s) {}^\tau \underline{V}_n^k}{\left\| h_k(r, s) {}^\tau \underline{V}_n^k \right\|}. \quad (2b)$$

For the director vectors in the spatial configuration also $\left\| {}^\tau \underline{V}_n^k \right\| = 1$.

In Eqn.(2a) ${}^\tau \lambda_o$ is a constant thickness stretching and ${}^\tau \lambda_1$ is the through-the-thickness stretching gradient.

In our formulation the element d.o.f. ${}^\tau \lambda_o$ and ${}^\tau \lambda_1$ are discontinuous across element boundaries and they will be condensed at the element level.

2.3 Incremental displacements

The incremental displacements to evolve from the τ -configuration to the $\tau + \Delta\tau$ -configuration are,

$$\underline{u} = {}^{\tau+\Delta\tau} \underline{x} - {}^\tau \underline{x} \quad (3a)$$

$$\begin{aligned} \underline{u}(r, s, t) &= h_k(r, s) \underline{u}_k \\ &+ \frac{t}{2} a ({}^\tau \lambda_o + \Delta\lambda_o + {}^\tau \lambda_1 t + \Delta\lambda_1 t) \frac{h_k(r, s) {}^{\tau+\Delta\tau} \underline{V}_n^k}{\left\| h_k(r, s) {}^{\tau+\Delta\tau} \underline{V}_n^k \right\|} \\ &- \frac{t}{2} a ({}^\tau \lambda_o + {}^\tau \lambda_1 t) \frac{h_k(r, s) {}^\tau \underline{V}_n^k}{\left\| h_k(r, s) {}^\tau \underline{V}_n^k \right\|}. \end{aligned} \quad (3b)$$

In the above, $\tau^{+\Delta\tau}\lambda_o = \tau\lambda_o + \Delta\lambda_o$ and $\tau^{+\Delta\tau}\lambda_1 = \tau\lambda_1 + \Delta\lambda_1$.

For the director vector rotations we can write [27],

$$\tau^{+\Delta\tau}\underline{V}_n^k = \tau^{+\Delta\tau}\underline{R} \cdot \tau\underline{V}_n^k \quad (4a)$$

with,

$$\tau^{+\Delta\tau}\underline{R} = \underline{I}_3 + \frac{\sin\theta_k}{\theta_k}\underline{\Theta}^k + \frac{1}{2}\left[\frac{\sin(\theta_k/2)}{(\theta_k/2)}\right]^2\left(\underline{\Theta}^k\right)^2. \quad (4b)$$

Using as base vectors $(\tau\underline{V}_1^k; \tau\underline{V}_2^k; \tau\underline{V}_n^k)$ defined as,

$$\tau\underline{V}_1^k = \frac{\tau\underline{e}_y \times \tau\underline{V}_n^k}{\left\|\tau\underline{e}_y \times \tau\underline{V}_n^k\right\|} \quad (4c)$$

$$\tau\underline{V}_2^k = \tau\underline{V}_n^k \times \tau\underline{V}_1^k \quad (4d)$$

where $\tau\underline{e}_y$ is the y -base vector at time τ of the fixed cartesian system in Fig.

1. We use a special definition for the case $\tau\underline{e}_y \times \tau\underline{V}_n^k = 0$ [8]:

$$\tau\underline{V}_1^k = \tau\underline{e}_z \quad (4e)$$

$$\tau\underline{V}_2^k = \tau\underline{e}_x \quad (4f)$$

Also,

$$\theta_k = \left[(\alpha_k)^2 + (\beta_k)^2\right]^{\frac{1}{2}} \quad (4g)$$

$$[\underline{\Theta}^k] = \begin{bmatrix} 0 & 0 & \beta_k \\ 0 & 0 & -\alpha_k \\ -\beta_k & \alpha_k & 0 \end{bmatrix}. \quad (4h)$$

Then we write Eqn. (4a) as in Ref. [27],

$$\tau^{+\Delta\tau}\underline{V}_n^k = \tau\underline{V}_n^k - \alpha_k \tau\underline{V}_2^k + \beta_k \tau\underline{V}_1^k - \frac{1}{2}\left[(\alpha_k)^2 + (\beta_k)^2\right]^\tau \underline{V}_n^k + h.o.t. \quad (5)$$

Hence,

$$\begin{aligned}
\underline{u} = & h_k \underline{u}_k + \frac{t}{2} \frac{a}{\left\| h_k \tau \underline{V}_n^k \right\|} (\tau \lambda_o + \tau \lambda_1 t) h_k (-\alpha_k \tau \underline{V}_2^k + \beta_k \tau \underline{V}_1^k) \quad (6) \\
& - \frac{t}{4} \frac{a}{\left\| h_k \tau \underline{V}_n^k \right\|} (\tau \lambda_o + \tau \lambda_1 t) h_k \left[(\alpha_k)^2 + (\beta_k)^2 \right] \tau \underline{V}_n^k \\
& + \frac{t}{2} \frac{a}{\left\| h_k \tau \underline{V}_n^k \right\|} (\Delta \lambda_o + \Delta \lambda_1 t) h_k \tau \underline{V}_n^k \\
& + \frac{t}{2} \frac{a}{\left\| h_k \tau \underline{V}_n^k \right\|} (\Delta \lambda_o + \Delta \lambda_1 t) h_k (-\alpha_k \tau \underline{V}_2^k + \beta_k \tau \underline{V}_1^k) \\
& - \frac{t}{4} \frac{a}{\left\| h_k \tau \underline{V}_n^k \right\|} (\Delta \lambda_o + \Delta \lambda_1 t) h_k \left[(\alpha_k)^2 + (\beta_k)^2 \right] \tau \underline{V}_n^k \\
& + h.o.t.
\end{aligned}$$

where, to simplify the formulation, we made the approximation,

$$\left\| h_k \tau + \Delta \tau \underline{V}_n^k \right\| \approx \left\| h_k \tau \underline{V}_n^k \right\|. \quad (7)$$

2.4 Strains interpolation

We can write the Green-Lagrange strain tensor as,

$$\tau \underline{\underline{\varepsilon}} = \tau \tilde{\varepsilon}_{IJ} \mathring{\underline{g}}^I \mathring{\underline{g}}^J \quad (8)$$

where,

$\tau \tilde{\varepsilon}_{IJ}$: covariant components in the element natural coordinate system,

$\mathring{\underline{g}}^I$: contravariant base vectors of the element natural coordinate system in the reference configuration,

$\mathring{\underline{g}}^I \mathring{\underline{g}}^J$: tensor product of the two contravariant base vectors [28].

We use, following the MITC4 interpolation [11] for the in-layer strain components,

$$\tau \tilde{\varepsilon}_{rr} = [\tau \tilde{\varepsilon}_{rr}]^{DI} \quad (9a)$$

$$\tau \tilde{\varepsilon}_{ss} = [\tau \tilde{\varepsilon}_{ss}]^{DI} \quad (9b)$$

$$\tau \tilde{\varepsilon}_{rs} = [\tau \tilde{\varepsilon}_{rs}]^{DI} \quad (9c)$$

In the above equations $[\tilde{\varepsilon}_{ij}]^{DI}$ are the strain components calculated from the displacement interpolation. In the same way, for the through-the-thickness strain component we use,

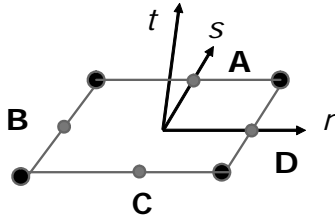


Figure 2: Sample points for the MITC4 transverse shear strain interpolations

$$\tau_{o\tilde{\varepsilon}tt} = [\tau_{o\tilde{\varepsilon}tt}]^{DI} \quad (9d)$$

and using the sample points indicated in Fig. 2 we interpolate the transverse shear strain components,

$$\tau_{o\tilde{\varepsilon}rt} = \frac{1}{2}(1+s) [\tau_{o\tilde{\varepsilon}rt}]_A^{DI} + \frac{1}{2}(1-s) [\tau_{o\tilde{\varepsilon}rt}]_C^{DI} \quad (9e)$$

$$\tau_{o\tilde{\varepsilon}st} = \frac{1}{2}(1+r) [\tau_{o\tilde{\varepsilon}st}]_D^{DI} + \frac{1}{2}(1-r) [\tau_{o\tilde{\varepsilon}st}]_B^{DI} . \quad (9f)$$

In the above equations $[\tilde{\varepsilon}_{ij}]_{SP}^{DI}$ are the strain components calculated from the displacement interpolation at the *sampling point* “*SP*”.

3 Hyperelastic constitutive relations

The shell element formulation developed in the previous section is a fully 3D formulation since the in-layer plane stress hypothesis used in the original MITC4 formulation was not invoked in this case.

There are many hyperelastic constitutive models available in the literature [29]. In order to explore the differences in their responses we implemented, for the new MITC4-3D shell element, three hyperelastic isotropic constitutive relations and we analyzed their responses for a number of finite strain cases.

3.1 Hooke's law relating 2nd Piola-Kirchhoff stresses and Green-Lagrange strains

In this case the elastic energy per unit volume of the reference (${}^{\circ}\mathcal{U}$) configuration is defined as [28],

$${}^{\tau}\mathcal{U} = \frac{1}{2} {}^{\tau}\underline{\underline{\varepsilon}} : \underline{\underline{C}} : {}^{\tau}\underline{\underline{\varepsilon}} \quad (10)$$

where ${}^{\tau}\underline{\underline{\varepsilon}}$ is the Green-Lagrange strain tensor [28] and $\underline{\underline{C}}$ is the isotropic Hooke's constitutive fourth order tensor [28].

Using the Doyle-Ericksen formula [28] we get,

$${}^{\tau}\underline{\underline{S}} = \underline{\underline{C}} : {}^{\tau}\underline{\underline{\varepsilon}} \quad (11)$$

where ${}^{\tau}\underline{\underline{S}}$ is the second Piola-Kirchhoff stress tensor [28].

Hooke's law establishes a linear relation between the deviatoric parts of the stress and strain measures and a linear relation between their hydrostatic parts. It should be noticed that, in this case, since for finite strains the hydrostatic part of the Green-Lagrange strain tensor does not represent the volumetric strain, the physics in Eqn. (11) is not obvious.

3.2 Compressible neo-Hookean model

We use the neo-Hookean model formulated in [30] where the elastic energy is split into a volumetric and a deviatoric part,

$${}^{\tau}\mathcal{U} = {}^{\tau}\mathcal{U}_v({}^{\tau}J) + {}^{\tau}\mathcal{U}_D({}^{\tau}\underline{\underline{b}}) . \quad (12)$$

In the above,

$${}^{\tau}J = \frac{{}^{\circ}\rho}{{}^{\tau}\rho} \quad (13a)$$

$${}^{\tau}\underline{\underline{b}} = ({}^{\tau}J)^{-\frac{2}{3}} {}^{\tau}\underline{\underline{b}} \quad (13b)$$

The second order tensor ${}^{\tau}\underline{\underline{X}}$ is the deformation gradient tensor; ${}^{\tau}\underline{\underline{b}} = {}^{\tau}\underline{\underline{X}} \cdot {}^{\tau}\underline{\underline{X}}^T$ is the Finger strain tensor and $({}^{\circ}\rho, {}^{\tau}\rho)$ are the densities in the reference and spatial configurations respectively. In Cartesian coordinates ${}^{\tau}J = \det [{}^{\tau}\underline{\underline{X}}]$ [28].

For the terms in Eqn. (12) Simo and Hughes use [30],

$${}^{\tau}\mathcal{U}_v({}^{\tau}J) = \frac{1}{2}\kappa \left[\frac{1}{2} \left[({}^{\tau}J)^2 - 1 \right] - \ln({}^{\tau}J) \right] \quad (13c)$$

$${}^{\tau}\mathcal{U}_D({}^{\tau}\underline{\underline{b}}) = \frac{1}{2} G \left[\text{tr}({}^{\tau}\underline{\underline{b}}) - 3 \right] = \frac{1}{2} G \left[\text{tr}({}^{\tau}\underline{\underline{C}}) - 3 \right] . \quad (13d)$$

Where,

$$\underline{\underline{\tau C}} = (\tau J)^{-\frac{2}{3}} \underline{\underline{\tau X}}^T \cdot \underline{\underline{\tau X}}$$

and,

$$\begin{aligned} \kappa &= \frac{E}{3(1-2\nu)} \text{ (compressibility modulus)} \\ G &= \frac{E}{2(1+\nu)} \text{ (shear modulus)} \\ E &: \text{ Young's modulus} \\ \nu &: \text{ Poisson's coefficient} \end{aligned}$$

Hence, using the Doyle-Ericksen formula and doing a push-forward [28] we get,

$$\underline{\underline{\tau T}} = \tau J \frac{d \underline{\underline{\tau U}}_v}{d \tau J} \underline{\underline{\tau g}} + 2 \operatorname{dev} \left[\underline{\underline{\tau X}} \cdot \frac{\partial \underline{\underline{\tau U}}_D}{\partial \underline{\underline{\tau C}}} \cdot (\underline{\underline{\tau X}})^T \right] \quad (14)$$

where $\underline{\underline{\tau T}}$ is the Kirchhoff stress tensor [28].

In this case the relation between the hydrostatic component of $\underline{\underline{\tau T}}$ and the volumetric stretch τJ is explicit.

3.3 Hooke's law relating the Hencky strain tensor and its energy conjugate stress tensor

In this case the elastic energy per unit volume of the reference configuration is defined as,

$$\tau \mathcal{U} = \frac{1}{2} \underline{\underline{\tau H}} : \underline{\underline{C}} : \underline{\underline{\tau H}} \quad (15)$$

where $\underline{\underline{\tau H}} = \ln \underline{\underline{\tau U}}$ is the Hencky or logarithmic strain tensor [28], $\underline{\underline{\tau U}}$ is the right stretch tensor and $\underline{\underline{C}}$ is the isotropic Hooke's constitutive fourth order tensor.

For an **isotropic** elastic material the stress measure energy-conjugate to the Hencky strain tensor is $\underline{\underline{\tau \Gamma}}$ with,

$$\underline{\underline{\tau \Gamma}}^{IJ} = [\underline{\underline{\tau R}}^* (\tau^{ij})]^{IJ} \quad (16)$$

in the above equation $[\underline{\underline{\tau R}}^* (\tau^{ij})]^{IJ}$ are the rotational pull-back of the contravariant components of the Kirchhoff stress tensor [28].

Using the Doyle-Ericksen formula we get,

$$\underline{\underline{\tau \Gamma}} = \underline{\underline{C}} : \underline{\underline{\tau H}}. \quad (17)$$

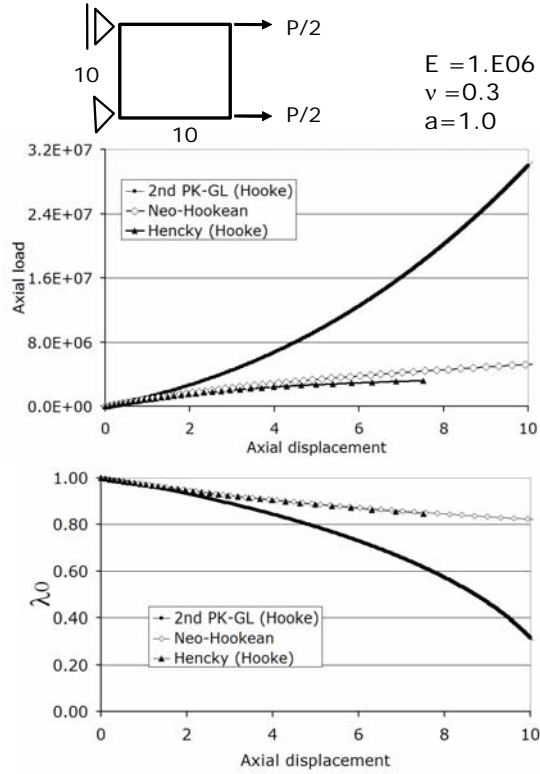


Figure 3: Plane stress axial test

It is important to notice that the hydrostatic part of the Hencky strain tensor is the logarithmic volumetric strain; hence, in this case the linear relation between the hydrostatic component of $\underline{\underline{T}}$ and the logarithmic volumetric strain has an obvious physical meaning.

For this constitutive relation we use the interpolations in Eqns. (9a) - (9f) but with the Hencky strain components instead of the Green - Lagrange strain components.

3.4 The behavior of the considered hyperelastic models

In order to explore the response that we can expect from the considered hyperelastic models, in Fig. 3 we analyze a simple plane-stress tension test.

It is obvious that except for very small axial displacements (infinitesimal strain situation) the three material models provide different responses, being the response of the first material model the most different while the responses of the other two models are close.

When dealing with a specific material only a laboratory test can indicate which hyperelastic law is the one that best approximates its behavior.

For metals undergoing finite elasto-plastic deformations, laboratory tests performed by Anand [31] indicate that using the standard values of the Young modulus and Poisson coefficient, the Hooke's law relating the Hencky strain tensor and its energy conjugate stress tensor provides the results that best approximate the actual material behavior for moderate elastic strains.

4 The incremental formulation

Using a total Lagrangian formulation we can write the Principle of Virtual Work for the equilibrium configuration at $\tau + \Delta\tau$ [8],

$$\int_{\circ V} \tau^{+\Delta\tau} S^{IJ} \delta \tau^{+\Delta\tau} \varepsilon_{IJ} \circ dV = \tau^{+\Delta\tau} \mathcal{R} \quad (18)$$

where $\tau^{+\Delta\tau} \mathcal{R}$ is the virtual work of the external loads acting on the solid body in the $\tau + \Delta\tau$ -configuration.

Now we can write [8],

$$\tau^{+\Delta\tau} S^{IJ} = \tau S^{IJ} + \circ S^{IJ} \quad (19a)$$

$$\tau^{+\Delta\tau} \varepsilon_{IJ} = \tau \varepsilon_{IJ} + \circ \varepsilon_{IJ} \quad (19b)$$

$$\circ \varepsilon_{IJ} = \circ e_{IJ} + \circ \eta_{IJ} \quad (19c)$$

where $\circ e_{IJ}$ is the increment in the Green-Lagrange strain tensor, linear in the incremental displacement and $\circ \eta_{IJ}$ is the nonlinear increment.

Using the incremental constitutive equation,

$$\circ S^{IJ} = \circ C^{IJKL} \circ \varepsilon_{KL} \quad (20)$$

we get the linearized incremental equation,

$$\int_{\circ V} \circ C^{IJKL} \circ e_{KL} \delta \circ e_{IJ} \circ dV + \int_{\circ V} \tau S^{IJ} \delta \circ \eta_{IJ} \circ dV = \tau^{+\Delta\tau} \mathcal{R} - \int_{\circ V} \tau S^{IJ} \delta \circ e_{IJ} \circ dV. \quad (21)$$

In what follows we develop Eqn. (21) for the three hyperelastic material models considered above.

4.1 First case: linear relation between 2nd Piola-Kirchhoff stresses and Green-Lagrange strains

We transform the components of the fourth order Hooke's constitutive tensor from a Cartesian system, with base vectors ${}^o\underline{e}_\alpha$, to the natural coordinate system, with covariant base vectors ${}^o\underline{\tilde{g}}_I$, using,

$$C^{\alpha\beta\gamma\delta} {}^o\underline{e}_\alpha {}^o\underline{e}_\beta {}^o\underline{e}_\gamma {}^o\underline{e}_\delta = \tilde{C}^{IJKL} {}^o\underline{\tilde{g}}_I {}^o\underline{\tilde{g}}_J {}^o\underline{\tilde{g}}_K {}^o\underline{\tilde{g}}_L. \quad (22)$$

Hence,

$${}^o\tilde{S}^{IJ} = \tilde{C}^{IJKL} {}^o\tilde{\varepsilon}_{KL} = \tilde{C}^{IJKL} ({}^o\tilde{e}_{KL} + {}^o\tilde{\eta}_{KL}) \quad (23)$$

and the linearized incremental equation is,

$$\int_{{}^oV} \tilde{C}^{IJKL} {}^o\tilde{e}_{KL} \delta {}^o\tilde{e}_{IJ} {}^o dV + \int_{{}^oV} {}^o\tilde{S}^{IJ} \delta {}^o\tilde{\eta}_{IJ} {}^o dV = \tau + \Delta\tau \mathcal{R} - \int_{{}^oV} {}^o\tilde{S}^{IJ} \delta {}^o\tilde{e}_{IJ} {}^o dV. \quad (24)$$

4.2 Second case: compressible neo-Hookean model

The components of the incremental constitutive tensor can be calculated from,

$${}^oC^{LMPQ} = 2 \frac{\partial {}^o\tau S^{LM}}{\partial {}^o\tau C_{PQ}} \quad (25)$$

where ${}^o\tau \underline{C} = {}^o\tau \underline{X}^T \cdot {}^o\tau \underline{X}$ is the Green strain tensor. The above derivative is calculated using Serrin formula [28] that for an isotropic material (${}^o\tau \underline{S}$ and ${}^o\tau \underline{C}$ are colinear tensors) can be written as,

$${}^o\tau S^{LM} = {}^o\tau S^I \left[(\tau \lambda_I)^2 \frac{{}^o\tau C_{LM} - \left(\tau I_C^1 - (\tau \lambda_I)^2 \right) {}^o g_{LM} + \tau I_C^3 (\tau \lambda_I)^{-2} ({}^o\tau C^{-1})_{LM}}{2 (\tau \lambda_I)^4 - \tau I_C^1 (\lambda_I)^2 + \tau I_C^3 (\tau \lambda_I)^{-2}} \right] \quad (26)$$

in the above,

$$\begin{aligned} {}^o\tau S^1 &= \frac{1}{(\tau \lambda_1)^2} \left[\frac{\kappa}{2} (\tau J^2 - 1) + G (\tau J)^{-2/3} \left(\frac{2(\tau \lambda_1)^2 - (\tau \lambda_2)^2 - (\tau \lambda_3)^2}{3} \right) \right] \\ {}^o\tau S^2 &= \frac{1}{(\tau \lambda_2)^2} \left[\frac{\kappa}{2} (\tau J^2 - 1) + G (\tau J)^{-2/3} \left(\frac{2(\tau \lambda_2)^2 - (\tau \lambda_1)^2 - (\tau \lambda_3)^2}{3} \right) \right] \\ {}^o\tau S^3 &= \frac{1}{(\tau \lambda_3)^2} \left[\frac{\kappa}{2} (\tau J^2 - 1) + G (\tau J)^{-2/3} \left(\frac{2(\tau \lambda_3)^2 - (\tau \lambda_1)^2 - (\tau \lambda_2)^2}{3} \right) \right] \end{aligned}$$

where ${}^\tau S^I$ are the eigenvalues of ${}^\tau \underline{\underline{S}}$ calculated using Eqn. (14) and doing a pull-back [28]; $({}^\tau \lambda_I)^2$ are the eigenvalues of $({}^\tau \underline{\underline{C}})$ and $({}^\tau I_C^1; {}^\tau I_C^2; {}^\tau I_C^3)$ are the invariants of ${}^\tau \underline{\underline{C}}$.

To calculate $\frac{\partial {}^\tau \lambda_I}{\partial {}^\tau C_{PQ}}$ we use the characteristic polynomial of the Green tensor [28] and calculate its derivative,

$$-({}^\tau \lambda_I)^6 + {}^\tau I_C^1 ({}^\tau \lambda_I)^4 - {}^\tau I_C^2 ({}^\tau \lambda_I)^2 + {}^\tau I_C^3 = 0 . \quad (27)$$

Of course we do not loose the hyperelastic symmetry, that is to say,

$${}_o C^{LMPQ} = {}_o C^{PQLM} . \quad (28)$$

After the above calculations we use the neo-Hookean incremental constitutive tensor in Eqns.(21).

4.3 Third case: linear relation between the Hencky strain tensor and its energy conjugate stress tensor

We define the fourth order tensor,

$${}^\tau D_{IJ}^{MN} = \frac{\partial {}^\tau H_{IJ}}{\partial {}^\tau \varepsilon_{MN}} . \quad (29)$$

To calculate the above defined tensor components we use again the Serrin formula. Using the tensor ${}^\tau \underline{\underline{D}}$ we can write,

$${}^\tau \tilde{\Gamma}^{IJ} = {}_o \tilde{C}^{IJKL} {}_o \tilde{H}_{KL} = {}_o \tilde{C}^{IJKL} \tilde{D}_{KL}^{MN} ({}_o \tilde{e}_{MN} + {}_o \tilde{\eta}_{MN}) . \quad (30)$$

Hence, the linearized incremental equation (21) can be written as,

$$\int_{oV} {}_o \tilde{C}^{IJKL} {}^\tau D_{IJ}^{PQ} {}^\tau D_{KL}^{RS} {}_o \tilde{e}_{PQ} \delta_o \tilde{e}_{RS} {}^o dV + \int_{oV} {}^\tau \tilde{\Gamma}^{IJ} {}^\tau D_{IJ}^{MN} \delta_o \tilde{\eta}_{MN} {}^o dV = \tau + \Delta \tau \mathcal{R} - \int_{oV} {}^\tau \tilde{\Gamma}^{IJ} {}^\tau D_{IJ}^{MN} \delta_o \tilde{e}_{MN} {}^o dV . \quad (31)$$

The resulting stiffness matrices are, of course, also symmetric.

5 Numerical studies

The d.o.f. $(\Delta \lambda_o, \Delta \lambda_1)$ are condensed at the element level and (20x20) element stiffness matrices are obtained and assembled into the global stiffness matrices.

5.1 Basic numerical studies

5.1.1 Convergence

The MITC4-3D shell element inherits from the MITC4 element the following properties:

- It does not contain spurious rigid body modes.
- It satisfies Irons' Patch Test.

5.1.2 Conditioning

In order to investigate the conditioning of the MITC4-3D element in Fig. 4 we compare, for a very thin element, the conditioning number of the stiffness matrices corresponding to a standard MITC4 element and to the new element. We use the conditioning number defined as [8],

$$\text{cond}(\underline{K}) = \log_{10} \frac{\Lambda_{\max}}{\Lambda_{\min}}. \quad (32)$$

In the above equation,

Λ_{\max} : maximum eigenvalue of the stiffness matrix,

Λ_{\min} : minimum non-zero eigenvalue of the stiffness matrix.

The comparison was performed considering the three defined hyperelastic constitutive relations and three different values of the Poisson coefficient. In the case of the MITC4-3D element the eigenvalues correspond to the condensed (20x20) stiffness matrix.

We see that the conditioning number of the MITC4-3D element is only slightly deteriorated in the case of an extreme value of the Poisson coefficient, as compared with the conditioning number of the standard MITC4 element.

5.2 Finite strain analyses

In this subsection we are going to analyze several cases of hyperelastic shells deforming into the finite strain regime.

For each case we consider the three hyperelastic constitutive models described above; hence, the purpose of this section is twofold: the investigation of the numerical performance of the MITC4-3D element formulation and the investigation of the differences in the shell structural responses corresponding to the three material models.

5.2.1 Cantilever under constant moment

In Fig. 5 we present the results for an elastic cantilever with $(L/a) = 100$, $E = 1.2E07$ and $\nu = 0.0$.

We obtain the same result for the three considered material models because the strains developed in the cantilever beam are only moderately high.

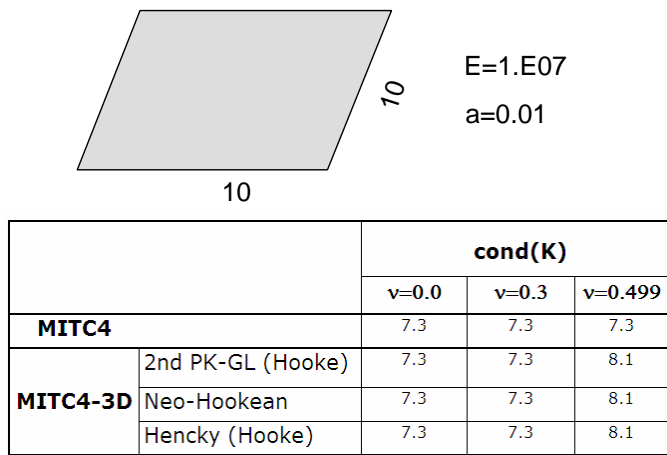


Figure 4: Conditioning of the MITC4-3D element compared with the conditioning of the MITC4 element

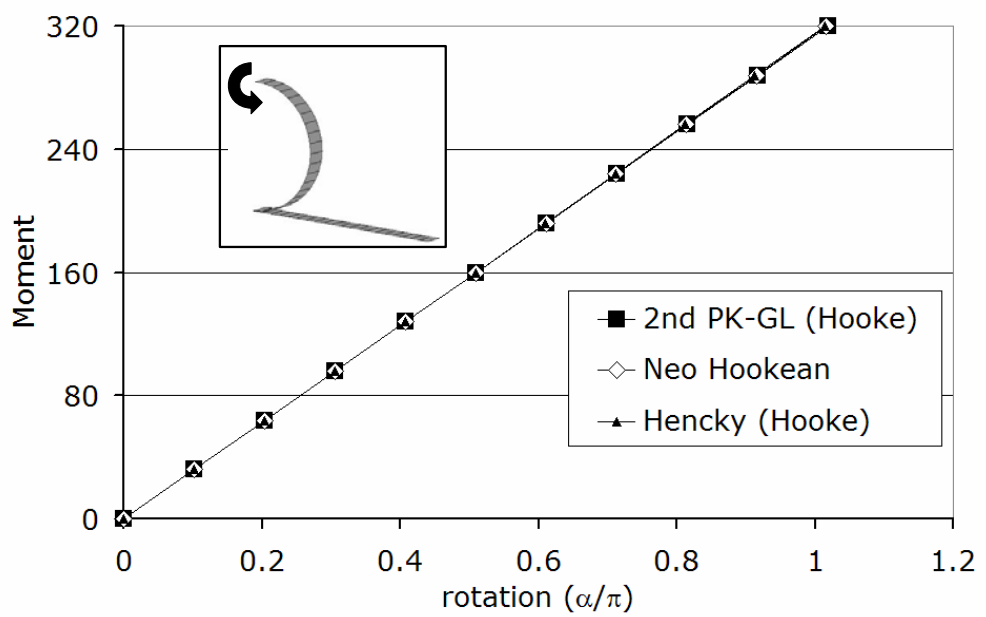


Figure 5: Elastic cantilever under constant moment ($L/a = 100$)

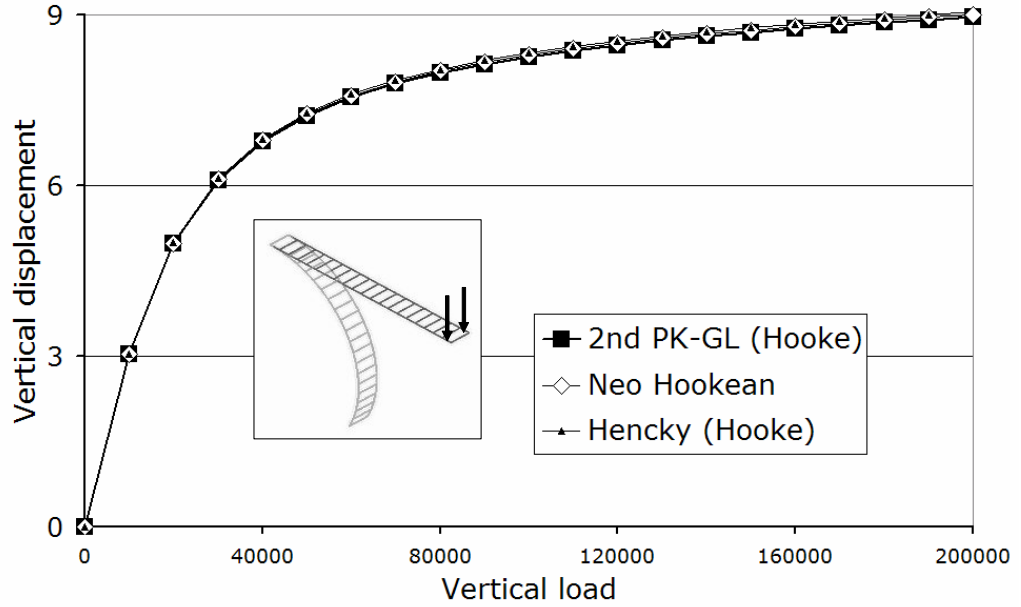


Figure 6: Vertical displacement of a cantilever under tip load (L/a) = 10

5.2.2 Cantilever under tip load

In Fig. 6 we present the results for the tip vertical displacement of an elastic cantilever with $(L/a) = 10$, $E = 1.2E07$ and $\nu = 0.3$.

Regarding the equilibrium path we obtain the same result for the three material models considered. In Fig. 7 we present the results for $(\tau \lambda_o, \tau \lambda_1)$ and in this case the results corresponding to the first constitutive relation are only slightly different from the results corresponding to the other two constitutive relations.

Again the reason for these very similar responses lies in the fact that the strains developed in the cantilever beam are only moderately high.

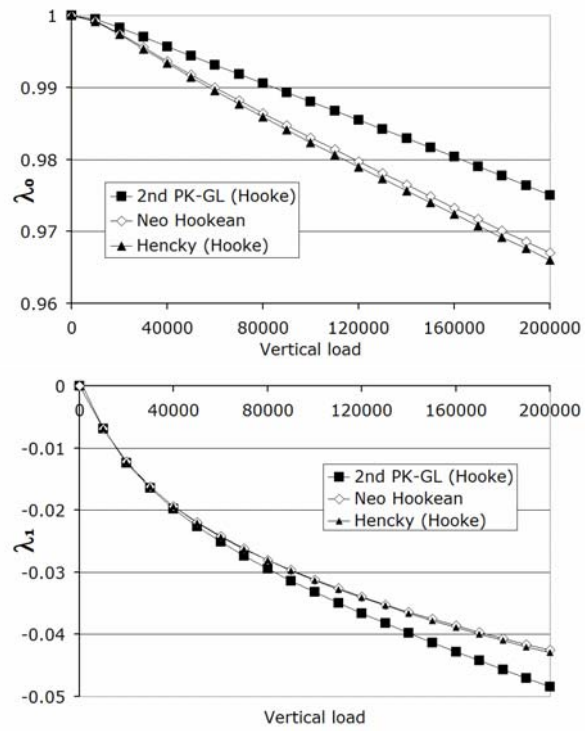


Figure 7: Cantilever under tip load $(L/a) = 10$. Through-the-thickness stretching in the element at the fixed boundary

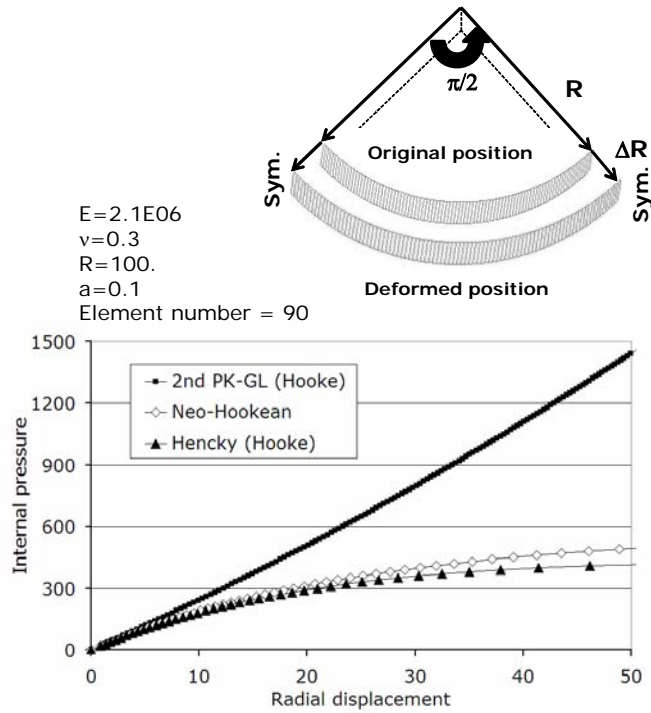


Figure 8: Infinite cylinder under internal pressure

5.2.3 Infinitely long cylinder under internal pressure

We consider the infinite cylinder represented in Fig. 8 under internal pressure. In the same figure we represent the equilibrium paths obtained for the infinitely long cylinder considering the three hyperelastic constitutive models discussed above. The strains developed in the cylinder wall are quite high; hence, the equilibrium paths are quite different, in particular the one corresponding to the first hyperelastic model.

Finally in Fig. 9 we present the predictions of the through-the-thickness stretching obtained with the three models considering two different values of the Poisson coefficient. Again the higher the strains the larger the difference between the structural responses predicted using the first constitutive model and the structural response predicted using any of the other two models.

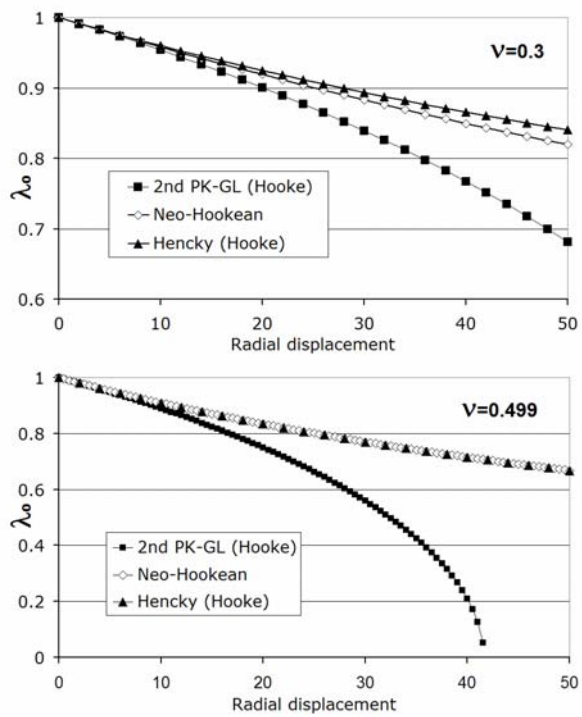


Figure 9: Infinitely long cylinder. Through-the-thickness stretching

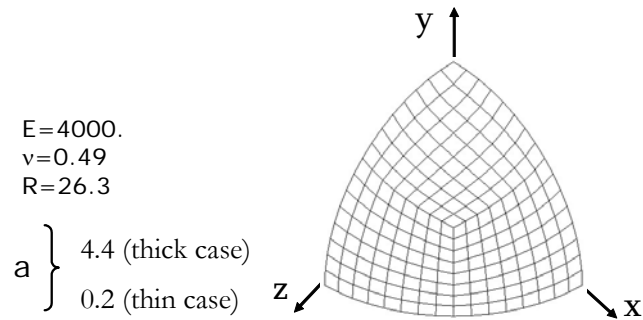


Figure 10: Sphere under internal pressure

5.2.4 Sphere under internal pressure

For the analysis of a sphere under internal pressure we consider two cases; a thick and a thin sphere, as it is shown in Fig. 10. For symmetry reasons only one eighth of the shell is modeled.

In Fig. 11 we present the results corresponding to the thick case; again, the first material model provides results that are quite different from the results provided by the other two material models.

In Fig. 12 we present the results corresponding to the thin case and the comment related to the behavior of the material constitutive models is again the same.

Notice that, as we should expect, when the thickness decreases $\lambda_1 \rightarrow 0$.

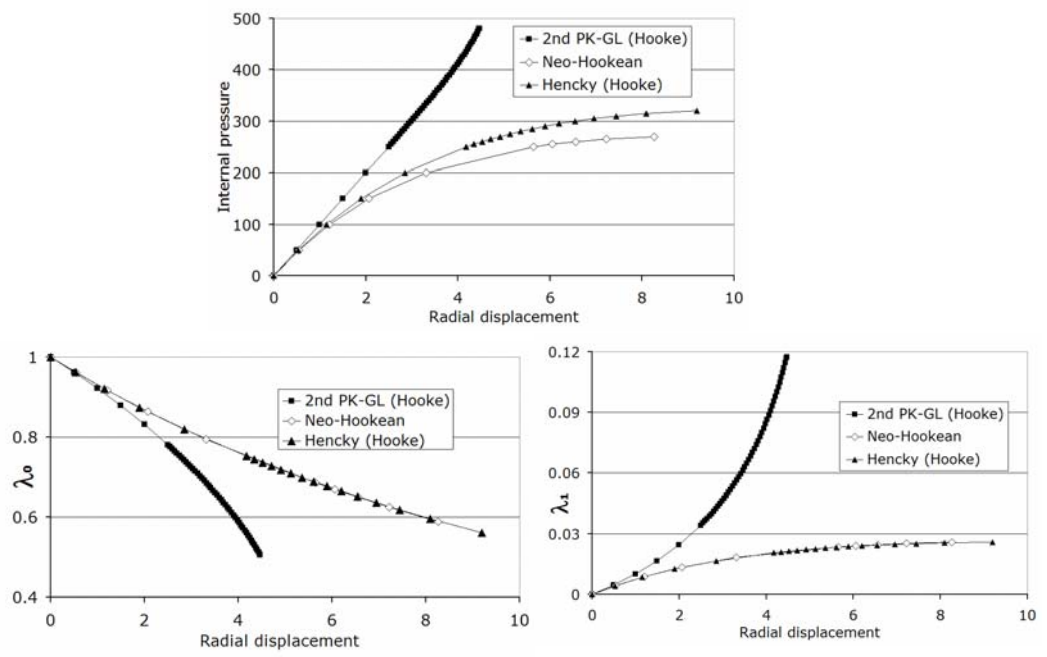


Figure 11: Sphere under internal pressure - thick case

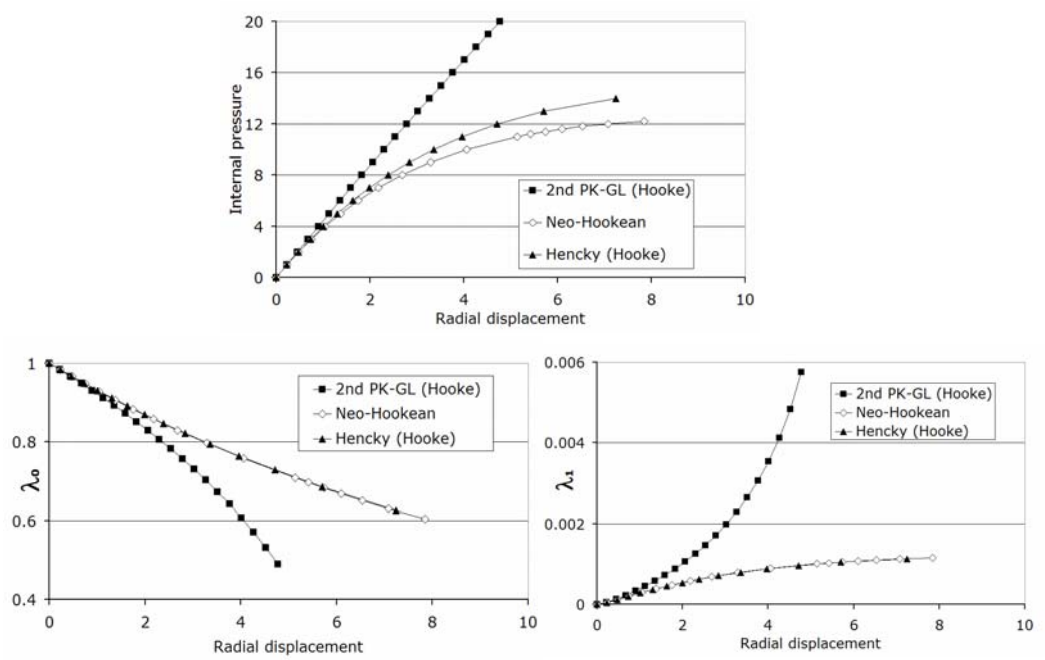


Figure 12: Sphere under internal pressure - thin case

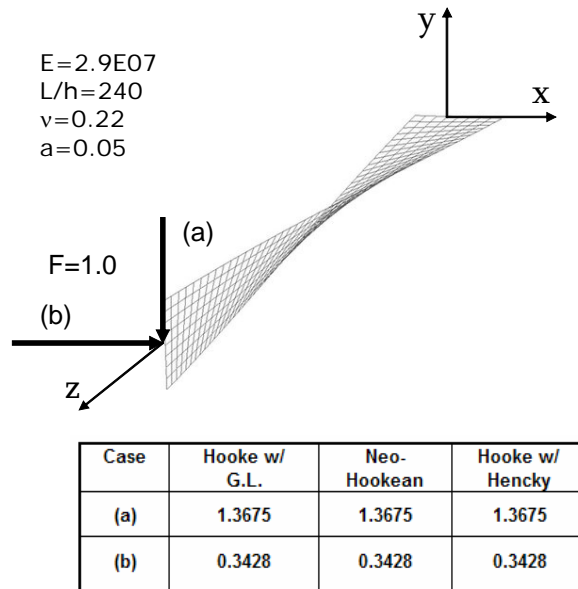


Figure 13: Twisted ribbon considering two load cases. Loaded point displacements

5.2.5 Twisted ribbon

For the two load cases represented in Fig. 13, in which the resulting strains are only moderate, the load displacements are identical considering the three material models.

5.2.6 Cylinder under line load

In Fig. 14 we describe the analyzed case.

In Figs. 15 and 16 we present the results obtained, for the three different hyperelastic constitutive relations.

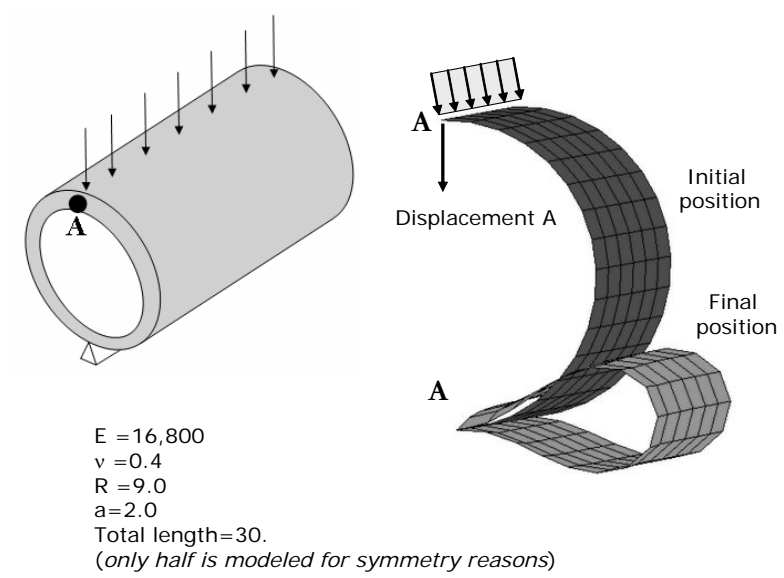


Figure 14: Cylinder under line load

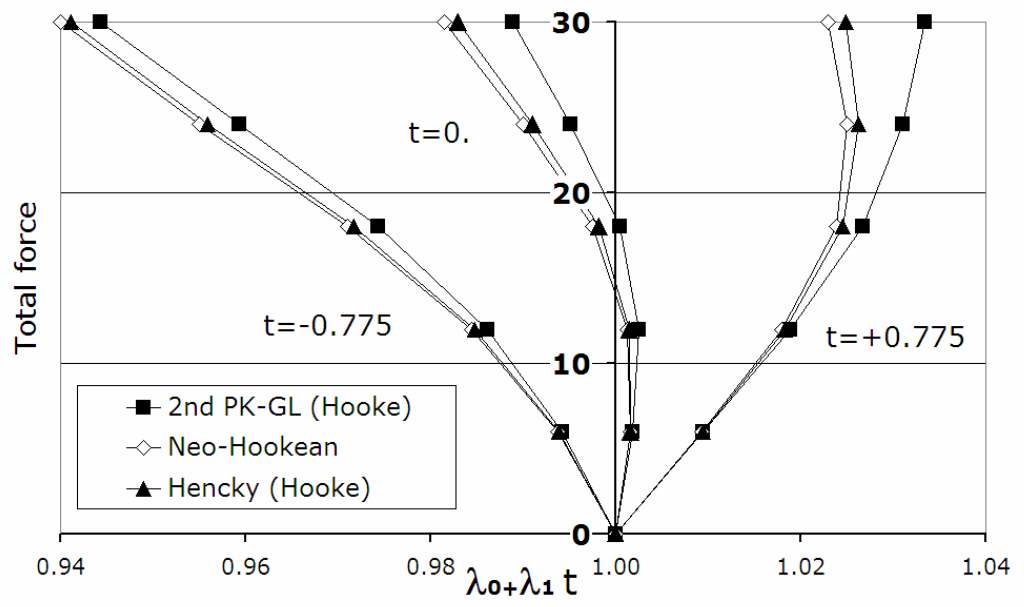


Figure 15: Thickness stretching at different depths for the element containing node A

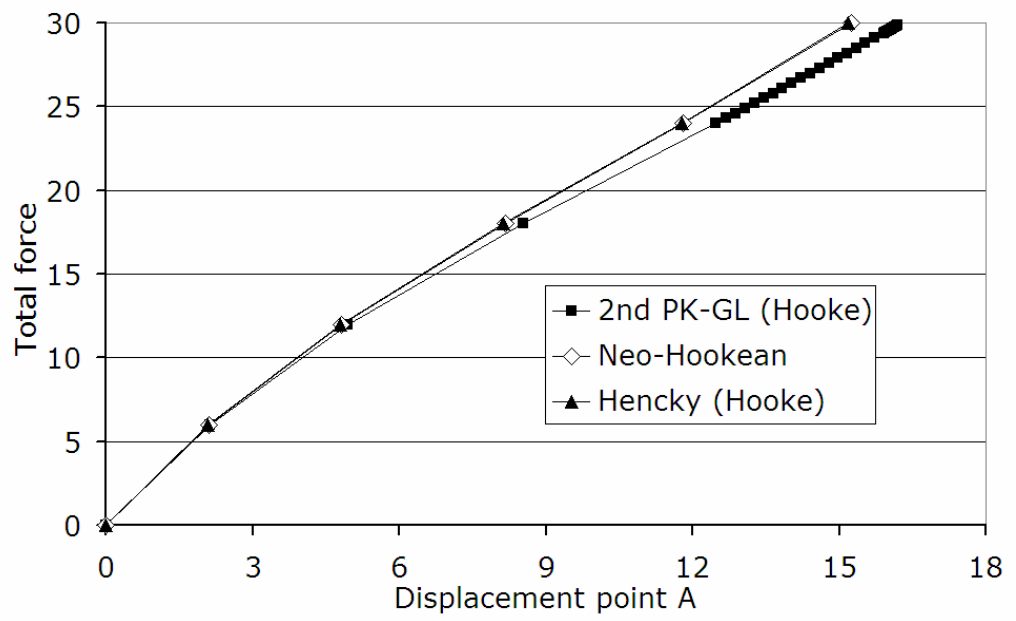


Figure 16: Load - displacement curves for the cylinder under line load

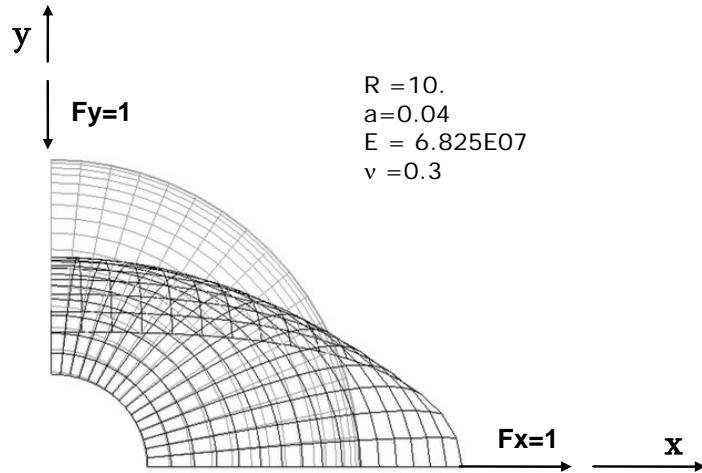


Figure 17: Pinched spherical shell with a 18° top hole

5.2.7 Pinched hemispherical shell

This case, depicted in Fig. 17, was used as a test case in many previous publications (e.g. [18]). It is a shell element with two opposite polar holes spanning a latitude of 18° each; for symmetry reasons only one eight of the shell is modeled.

The results obtained with the MITC4-3D element and the above described constitutive relations, using two different meshes, are presented in Fig. 18.

In this case the results corresponding to the three constitutive models converge to almost the same result when the mesh is refined.

6 Conclusions

On the basis of the MITC4 shell element formulation, we developed the MITC4-3D shell element formulation for finite strain analyses of shell structures using

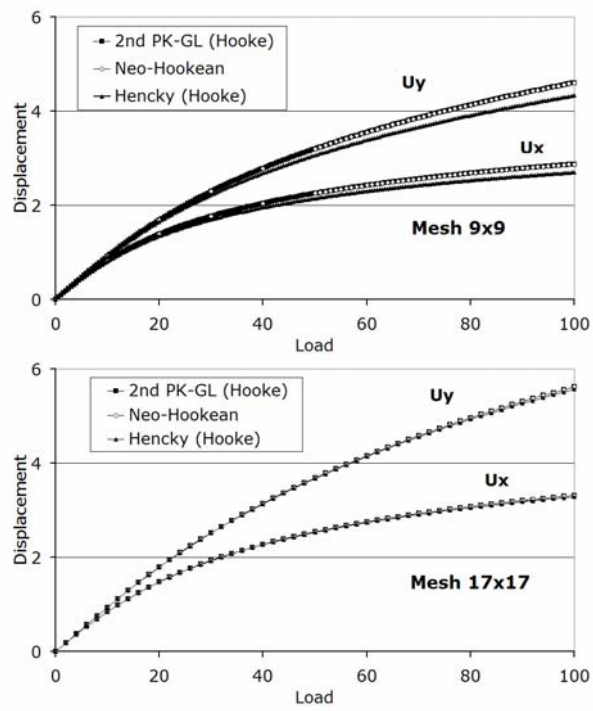


Figure 18: Pinched spherical shell results

general 3D constitutive models. In this paper the new element was implemented for the analyses of hyperelastic shell structures and the results indicate that it is a very effective element.

The results obtained considering three of the hyperelastic material models available in the literature are quite different when the developed strains are relatively high; this indicates that, for analyzing actual engineering examples, experimental data should be used to decide on the most suitable constitutive relation.

References

- [1] Ahmad S, Irons B.M. and Zienkiewicz O.C. (1970), "Analysis of thick and thin shell structures by curved finite elements", *Int. J. Numerical Methods in Engng.*, vol. 2, pp.419-451.
- [2] Ramm E. (1977), "A plate/shell element for large deflections and rotations", *Formulations and Computational Algorithms in Finite Element Analysis* (Eds. K.J. Bathe et al.), MIT Press, Cambridge, MA.
- [3] Kråkeland B. (1978), "Nonlinear analysis of shells using degenerate isoparametric elements", *Finite Elements in Nonlinear Mechanics* (Eds. P.G. Bergan et al.), Tapir Publishers, Norwegian Institute of Technology, Trondheim, Norway.
- [4] Bathe K.J. and Bolourchi S. (1980), "A geometric and material nonlinear plate and shell element", *Computers & Struct.*, vol. 11, pp. 23-48.
- [5] Zienkiewicz O.C., Taylor R.L. and Too J.M. (1971), "Reduced integration technique in general analysis of plates and shells", *Int. J. Numerical Methods in Engng.*, vol. 3, pp. 275-290.
- [6] Bathe K.J., Dvorkin E.N. and Ho L.W. (1983), "Our discrete-Kirchhoff and isoparametric shell elements for nonlinear analyses - an assessment", *Computers & Struct.*, vol. 16, pp.89-98.
- [7] Belytschko T., Stolarski H., Liu W.K., Carpenter N., and Ong J. (1985), "Stress projections for membrane and shear locking in shell finite elements", *Comput. Meth. Appl. Mech. Engng.*, vol. 51, pp. 221-258.
- [8] Bathe K.J. (1996), *Finite Element Procedures*, Prentice Hall, Upper Saddle River, NJ.
- [9] Zienkiewicz O.C. and Taylor R.L. (2000), *The Finite Element Method*, Vol. 2, 5th Edition, Butterworth-Heinemann.
- [10] Chapelle D. and Bathe K.J. (2003), *The Finite Element Analysis of Shells - Fundamentals*, Springer, Berlin.

- [11] Dvorkin E.N. and Bathe K.J. (1984), "A continuum mechanics based four-node shell element for general nonlinear analysis", *Engng. Computations*, vol. 1, pp. 77-88.
- [12] Bathe K.J. and Dvorkin E.N. (1985), "A four-node plate bending element based on Mindlin / Reissner plate theory and a mixed interpolation", *Int. J. Numerical Methods in Engng.*, vol. 21, pp. 367-383.
- [13] Bathe K.J. and Dvorkin E.N. (1986), "A formulation of general shell elements - the use of mixed interpolation of tensorial components", *Int. J. Numerical Methods in Engng.*, vol. 22, pp.697-722.
- [14] Rodal J.J.A. and Witmer E.A. (1979), "Finite-strain large-deflection elastic-viscoplastic finite-element transient analysis of structures", *NASA CR 159874*.
- [15] Hughes T.J.R. and Carnoy E. (1983), "Nonlinear finite element shell formulation accounting for large membrane strains", *Comput. Meth. Appl. Mechs. Engng.*, vol. 39, pp.69-82.
- [16] Simo J.C. and Fox D.D. (1989), "On a stress resultant geometrically exact shell model. Part I: Formulation and optimal parametrization", *Comput. Meth. Appl. Mechs. Engng.*, vol. 72, pp.267-304.
- [17] Simo J.C. , Fox D.D. and Rifai M.S. (1989), "On a stress resultant geometrically exact shell model. Part II: The linear theory; computational aspects", *Comput. Meth. Appl. Mechs. Engng.*, vol. 73, pp.53-92.
- [18] Simo J.C. , Fox D.D. and Rifai M.S. (1990), "On a stress resultant geometrically exact shell model. Part III: Computational aspects of the nonlinear theory", *Comput. Meth. Appl. Mechs. Engng.*, vol. 79, pp.21-70.
- [19] Simo J.C., Fox D.D. and Rifai M.S. (1992), "On a stress resultant geometrically exact shell model. Part IV: Variable thickness shells with through-the-thickness stretching", *Comput. Meth. Appl. Mechs. Engng.*, vol. 81, pp.91-126.
- [20] Simo J.C. and Kennedy J.G. (1992), "On a stress resultant geometrically exact shell model. Part V: Nonlinear plasticity formulation and integration algorithms", *Comput. Meth. Appl. Mechs. Engng.*, vol. 96, pp.133-171.
- [21] Büchter N., Ramm E. and Roehl D. (1994), "Three-dimensional extension of non-linear shell formulation based on the enhanced assumed strain concept", *Int. J. Numerical Methods in Engng.*, vol. 37, pp. 2551-2568.
- [22] Bischoff M. and Ramm E. (1997), "Shear deformable shell elements for large strains and rotations", *Int. J. Numerical Methods in Engng.*, vol. 40, pp. 4427-4449.

- [23] Dvorkin E.N., Pantuso D. and Repetto E.A. (1995), “A formulation of the MITC4 shell element for finite strain elasto-plastic analysis”, *Comput. Meth. Appl. Mechs. Engng.*, vol. 125, pp.17-40.
- [24] Dvorkin E.N. (1995), “Nonlinear analysis of shells using the MITC formulation”, *Archives Comput. Meth. Engng.*, vol. 2, pp.1-50.
- [25] Gebhardt H. and Schweizerhof K. (1993), “Interpolation of curved shell geometries by low order finite elements - Errors and modifications”, *Int. J. Numerical Methods in Engng.*, vol. 36, pp.287-302.
- [26] Dvorkin E.N. (1992), “On nonlinear analysis of shells using finite elements based on mixed interpolation of tensorial components”, published in *Non-linear Analysis of Shells by Finite Elements*, (Ed. F.G. Rammerstorfer), CISM Courses and Lectures No. 328, Springer - Verlag, Wien - New York.
- [27] Dvorkin E.N., Oñate E. and Oliver J. (1988), “On a nonlinear formulation for curved Timoshenko beam elements considering large displacement/rotation increments”, *Int. J. Numerical Methods in Engng.*, vol. 26, pp. 1597-1613.
- [28] Dvorkin E.N. and Goldschmit M.B. (2005), *Nonlinear Continua*, Springer, Berlin.
- [29] Ogden R.W. (1997) , *Non-linear Elastic Deformations*, Dover.
- [30] Simo J.C. and Hughes T.J.R. (1998), *Computational Inelasticity*, Springer, New York.
- [31] Anand L. (1979), “On Hencky’s approximate strain-energy function for moderate deformations”, *J. Appl. Mech.*, vol. 46, pp.78-82.